Two-phase wake-mixing layer flow past a splitter plate: an experimental investigation

Della Pia, A.; Michelis, Theodorus; Chiatto, Matteo; Kotsonis, M.; de Luca, Luigi

DOI
10.2514/6.2023-3774

Publication date
2023

Document Version
Final published version

Published in
AIAA AVIATION 2023 Forum

AIAA AVIATION Forum
12-16 June 2023, San Diego, CA and Online
AIAA AVIATION 2023 Forum

10.2514/6.2023-3774

Two-phase wake-mixing layer flow past a splitter plate: an experimental investigation

Alessandro Della Pia *, Theodoros Michelis†, Matteo Chiatto‡, Marios Kotsonis§ and Luigi de Luca¶

The wake-mixing layer flow developing past a splitter plate separating two parallel gas and liquid co-flowing currents is experimentally investigated in this work. Time-resolved particle image velocimetry (TR-PIV) measurements of the two-phase velocity field are simultaneously performed in gas and liquid streams, shedding light on both mean (time-averaged) and unsteady features of the flow configuration. A selected reference case is first analyzed, revealing the presence of a wake region within the flow field, right behind the splitter plate. By progressively moving downstream along the streamwise x direction, a pure mixing layer region is retrieved. The effect of two governing flow parameters, namely the gas Reynolds number Re_g and the gas-liquid dynamic pressure ratio M, is then investigated, focusing first on the mean flow topology. It is found that the streamwise extension of the wake x_w is a monotonic decreasing function of Re_g, and it vanishes for the highest Re_g value considered, the two-phase flow resulting in a pure mixing layer regime. The flow unsteady development is then characterized by means of the spectral analysis of normal-to-flow (i.e. along y direction) velocity fluctuating quantities $v'(t)$, performed in both gas and liquid flows. As major results, it is found that frequency spectra are characterized by a high frequency content in the low Re_g configuration, the peak frequency depending on the streamwise location x. On the other hand, by progressively increasing Re_g the peak frequency shifts to lower values, and it becomes independent on the specific spatial location by increasing M. It is found that, at high Re_g and M values, velocity fluctuations are characterized by low frequency temporal oscillations synchronized over a large spatial extent of the flow field. The different regimes outlined by variation of the flow governing parameters are found to be consistent with convective/absolute instability behaviors highlighted by spatio-temporal linear stability analyses of the flow recently presented in literature.

I. Introduction

The wake-mixing layer flow developing past a splitter plate separating two parallel gas and liquid co-flowing currents is experimentally investigated in this work. The topic is relevant for both technological and scientific aspects. From one hand, two-phase mixing layer flow configurations are encountered in industrial air-blast atomizers, such as liquid fuel injectors in combustion engines. In these applications, a relatively low-speed liquid jet interacts with a faster parallel co-flowing gaseous phase downstream of a separator (or splitter) plate, which initially separates the fluids (Raynal et al. [1], Ben Rayana et al. [2], Eggers and Villermaux [3]). Among many others, the application of such a flow configuration to model the fuel injection in aeronautical engines, where the quality of combustion and then pollutant generation crucially depend on the characteristics of the atomization process (Lefebvre [4]), makes the topic of primary interest for both automotive and aerospace industrial sectors. On the other hand, disclosing the physical mechanisms which underlie the different stages of the interfacial instability characterizing two-phase mixing layers is a matter of active scientific research nowadays (Ling et al. [5], Jiang and Ling [6], Bozonnet et al. [7]). As a matter of fact, the velocity difference existing between the two phases meeting at the splitter plate edge triggers a shear instability at the separating interface, which leads to the generation of waves in the liquid phase. These waves are in turn affected by secondary instabilities, determining the formation, corrugation and finally breaking of ligaments into droplets (primary atomization). The process leads to the generation of mutually interacting gas-droplets mixtures, in the so-called secondary atomization, representing the last stage of the *instability cascade* (Marmottant and Villermaux [8]). Among other goals, further improving the comprehension of the instability cascade is of crucial importance to enhance the modeling and control of two-phase mixing layer flows.

*Ph.D. candidate, Department of Industrial Engineering, University of Naples Federico II, Naples 80125, Italy.
†Post-doc researcher, Section of Aerodynamics, Delft University of Technology, Delft, 2629HS, The Netherlands.
‡Assistant Professor, Department of Industrial Engineering, University of Naples Federico II, Naples 80125, Italy.
§Associate Professor, Section of Aerodynamics, Delft University of Technology, Delft, 2629HS, The Netherlands.
¶Professor, Department of Industrial Engineering, University of Naples Federico II, Naples 80125, Italy.

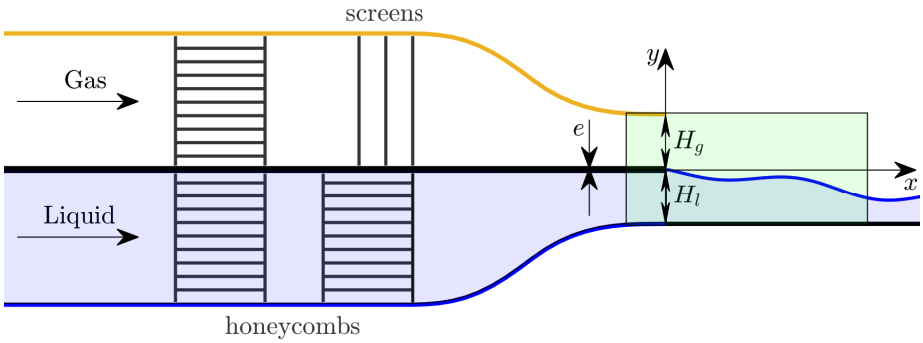

Fig. 1 Two-dimensional sketch of the two-phase mixing layer experimental setup close to the nozzle exit section. The PIV measurement region of interest is highlighted in green.

The present study focuses on the early stages of the primary instability of the gas-liquid mixing layer interface, and it aims at investigating the peculiar features of the complex wake-mixing layer flow which establishes just downstream of the splitter plate. In particular, an experimental characterization of the flow by means of two-components time-resolved particle image velocimetry (TR-PIV) is provided, performing flow field measurements simultaneously in gas and liquid streams. This kind of measurement is particularly challenging, due to several issues related to the presence of two different flow phases, such as undesirable laser light reflections at the gas-liquid interface, and the huge difference (two order of magnitude) in the two phases injection velocities (Sanchis and Jensen [9], Ayati et al. [10], Andrè and Bardet [11], Buckley and Veron [12], Kosiwczuk et al. [13]). By means of a proper light sheet optics arrangement, a single-laser single-camera measuring configuration is employed in this work. The two-phase mean velocity field is first characterized for a selected reference configuration, and then investigated by variation of flow governing parameters related to both gas (U_g) and liquid (U_l) injection velocities, namely the gas Reynolds number (Re_g) and the gas-liquid dynamic pressure ratio (M). Finally, the unsteady development of the flow is investigated by means of the spectral analysis of velocity fluctuating quantities, discussing results in comparison with previous findings of literature.

II. Methodology

A two-dimensional sketch of the experimental apparatus employed to study the two-phase mixing layer flow is reported in Fig. 1, focusing in particular on the near-field flow region, i.e. immediately after the nozzle exit section. A water stream flows along the streamwise x direction below a parallel co-flowing faster air current, the two fluids being separated by a stainless steel splitter plate with thickness equal to $e = 2$ mm. The shape of water and air channels is the same: walls are made in Plexiglas, the cross-sectional area is initially 100×100 mm^2, then a two-dimensional converging nozzle reduces the channels height from 100 mm to $H_g = H_l = 20$ mm at $x = 0$, where the flows issue into a test section. The injection flow velocities (i.e. at the splitter plate edge location, $x = 0$) are denoted as U_l and U_g, respectively for the liquid and gas currents. Particular care is taken in designing the flow conditioners for the gas phase (honeycombs and anti-turbulence screens), in order to keep the gas flow turbulence intensity level below 1% for all the experiments realized.

A single-laser single-camera measurement system is employed to achieve the PIV characterization of the flow simultaneously in the two phases. A Continuum Mesa PIV 532-120M laser with pulse at 2 kHz repetition rate (pulse energy 18 mJ) is used to generate a light beam, which is then separated in two different beams by a prism. A first beam goes through a combination of two spherical and one cylindrical lenses and a mirror, thus becoming a thin sheet enlightening the liquid phase. A second beam is rotated horizontally by a mirror, and it is transformed into an analogous sheet for the air flow by the same combination of lenses and mirror. A high speed (2 kHz repetition rate in double exposure mode) camera (Photron, Fastcam SA-1, 1024 × 1024 pixels) and a programmable timing unit (LaVision, HSC) complete the measurement setup. Liquid particles (mean diameter 1 μm) are seeded in the air channel by a fog generator (SAFEX, Fog 2010+) using a working fluid of water–glycol mixture, while a 20 μm polyamide Vestosint powder is used to seed the liquid phase.

A field of view equal to $[-18, 108] \times [-21, 21]$ mm^2 (qualitatively represented by the green region in Fig. 1) is imaged by mounting a 105 mm objective (Nikon, Micro-Nikkor) on the high-speed camera, thus giving a two-dimensional region of interest within the xy plane positioned midway from the channel side walls. By adjusting the camera focus,

Case	LO	REF	HI	HI-M
Re_g	384	493	768	768
M	1.31	2.57	11.81	25.56
U_g (m/s)	5	7	15	15
U_l (m/s)	0.15	0.15	0.15	0.10

Table 1 Overview of the cases considered in the analysis. Dimensionless parameters Re_g and M are defined in Eq. (2).

particle images approximately 2–3 px in diameter are obtained in both liquid and gas phases. An algorithm written in MATLAB is used to pre-process the raw images and separate the air and water phases, which are then post-processed separately through LaVision Davis 10. An iterative multi-grid cross-correlation scheme with window deformation (Scarano and Riethmuller [14]) is used to compute velocity fields, and results are post-processed with the universal outlier detection algorithm (Westerweel and Scarano [15]). For each couple of U_g and U_l values considered, the time delay Δt_l for cross-correlation in water is simply adjusted by skipping the number of frames necessary to achieve the same peak particle displacement as in air, i.e. $U_l \Delta t_l = U_g \Delta t_g$. The mean velocity components $\bar{u}$ and $\bar{v}$ are computed as

$$\bar{u}(x,y) = \frac{\sum_{j=1}^{N} u_j(x,y,t_j)}{N_t}, \quad \bar{v}(x,y) = \frac{\sum_{j=1}^{N} v_j(x,y,t_j)}{N_t}, \tag{1}$$

where u and v are the instantaneous measured velocity components along x and y directions, respectively, and $N_t = 8000$ is the total number of temporal realizations of the flow. Note that the spatial coordinates x and y have been made dimensionless by means of the splitter plate thickness e.

III. Time-averaged flow field analysis

The two-phase mixing layer flow configuration is analyzed by variation of its dimensionless governing parameters, namely the gas Reynolds number Re_g and the gas-liquid dynamic pressure ratio M, respectively defined as

$$Re_g = \frac{\rho_g U_g \delta_g}{\mu_g}, \quad M = \frac{\rho_g U_g^2}{\rho_l U_l^2}, \tag{2}$$

where ρ_g (ρ_l) is the gas (liquid) density, μ_g the gas dynamic viscosity, and δ_g the gas vorticity thickness. An overview of the analyzed experimental conditions is reported in Table 1, which specifies the cases considered (LO, REF, HI and HI-M) in terms of corresponding Re_g, M, U_g and U_l values. The first three cases are characterized by the same value of the liquid injection velocity ($U_l = 0.15$ m/s) and progressively increasing gas velocities U_g, from the LO (low Re_g) to the HI (high Re_g) case. The last case (HI-M) is obtained by decreasing the liquid velocity down to $U_l = 0.10$ m/s, so as to increase the dynamic pressure ratio parameter up to $M = 25.56$ at fixed $Re_g = 768$. Note also that all experiments have been designed so as to work at a relatively high plate to gas vorticity thickness ratio (i.e. $e/\delta_g > 1$), namely in the so called injector influenced regime identified by Fuster et al. [16].

The time-averaged velocity magnitude $\bar{V}$ contour of the REF case is shown in Fig. 2(a) together with the velocity vectors distribution, and a zoom around the splitter plate immediately downstream of the nozzle exit section is provided in Fig. 2(b). In both panels, the time-averaged interface location is represented as a white dashed line, and the velocity magnitude has been scaled with respect to the reference value U_g. Note also that, here and elsewhere, velocity vectors in the liquid phase have been magnified by a factor of $O(10^2)$. After issuing from the injection section ($x = 0$), the air and water flows meet downstream of the splitter plate. By moving along the streamwise direction, two distinct regions can be detected: a wake flow region ($0 < x < x_w$), and a pure mixing layer region ($x > x_w$), with $x_w = 17.5$. The wake region length x_w has been calculated as the last streamwise station (starting from $x = 0$) where $\bar{u}(y) < 0$ (i.e. $\bar{u} > 0$ for $x > x_w$). The spatial development of the mixing layer is more clearly quantified in Fig. 3, which reports $\bar{u}(y)$ profiles at different streamwise stations, spanning both air and water streams. Note that, for each spatial location, the average measurement uncertainty is also represented by means or error bars. The reverse flow component within the wake

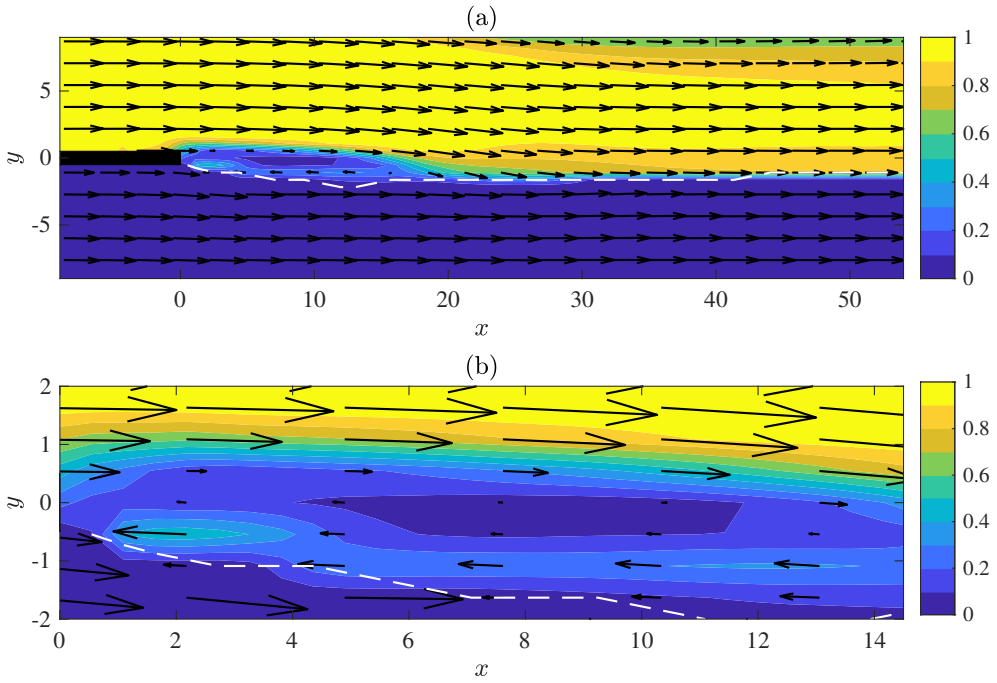

Fig. 2 Time-averaged velocity magnitude $\bar{V}/U_g$ contour (a) with zoom next to the splitter plate edge (b). The plate is highlighted in black, the time-averaged interface location is represented as a white dashed line, and velocity vectors are also reported. REF case of Table 1.

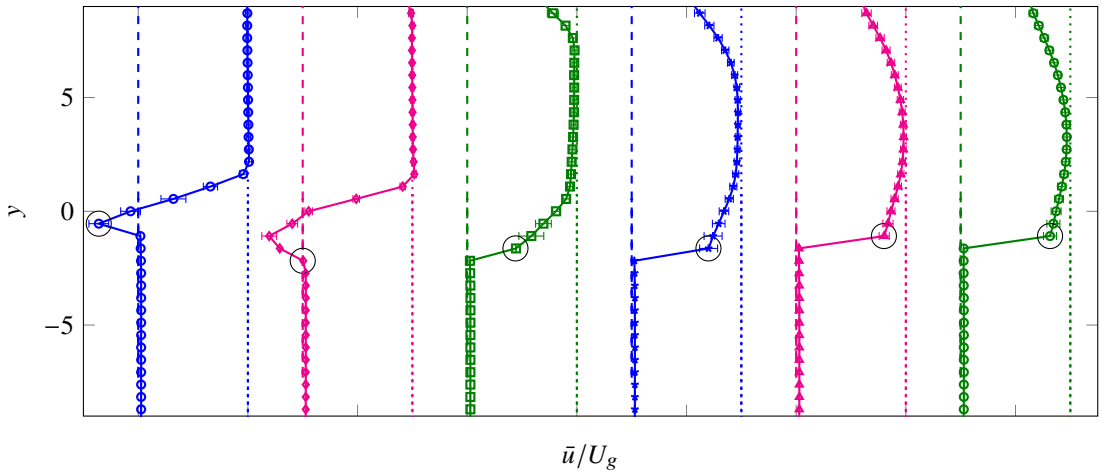

Fig. 3 Time-averaged streamwise $\bar{u}(y)/U_g$ velocity component profiles at different x stations: x = 0.55 (—o—); 10.88 (—◇—); 21.76 (—□—); 32.10 (—☆—); 42.98 (—△—); 53.31 (—○—). The dashed and dotted lines represent the values $\bar{u}/U_g$ = 0 and 1, respectively, error bars denote the average measurement uncertainty, while black circles highlight the interface location. REF case of Table 1.

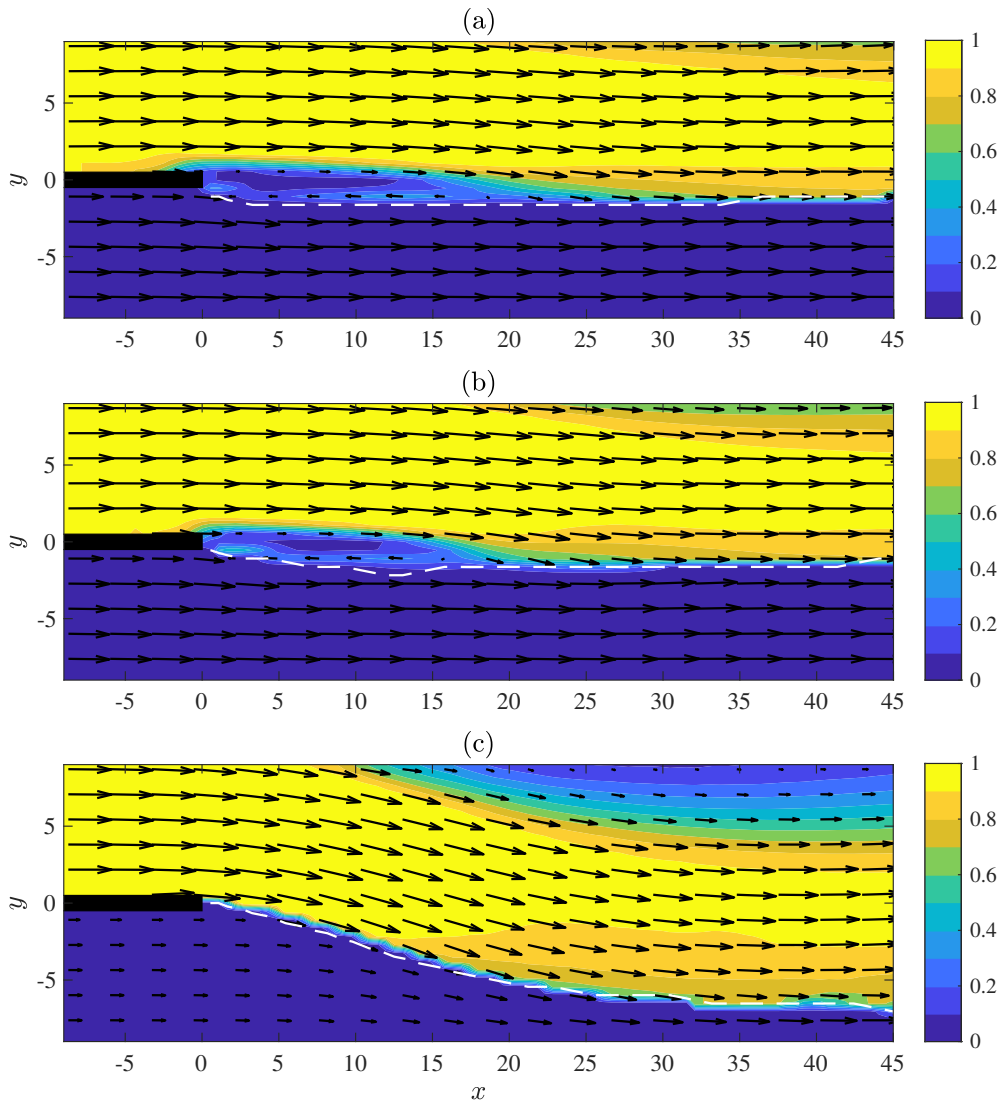

Fig. 4 Reynolds number Re_g effect on the time-averaged velocity magnitude $\bar{V}/U_g$. The splitter plate is highlighted in black, the time-averaged interface location is represented as a white dashed line, and velocity vectors are also reported. LO (a), REF (b) and HI (c) cases of Table 1.

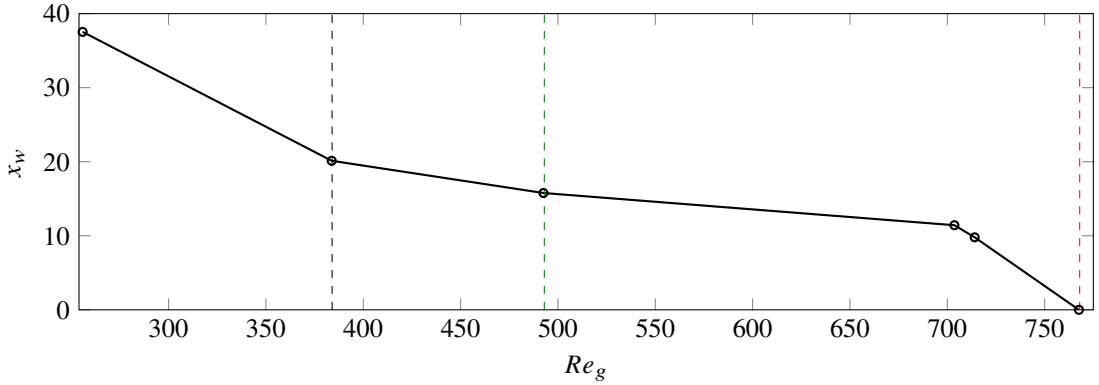

Fig. 5 Reynolds number Re_g effect on the wake region length x_w. The vertical dashed lines denote the LO (black), REF (green) and HI (red) cases of Table 1, respectively.

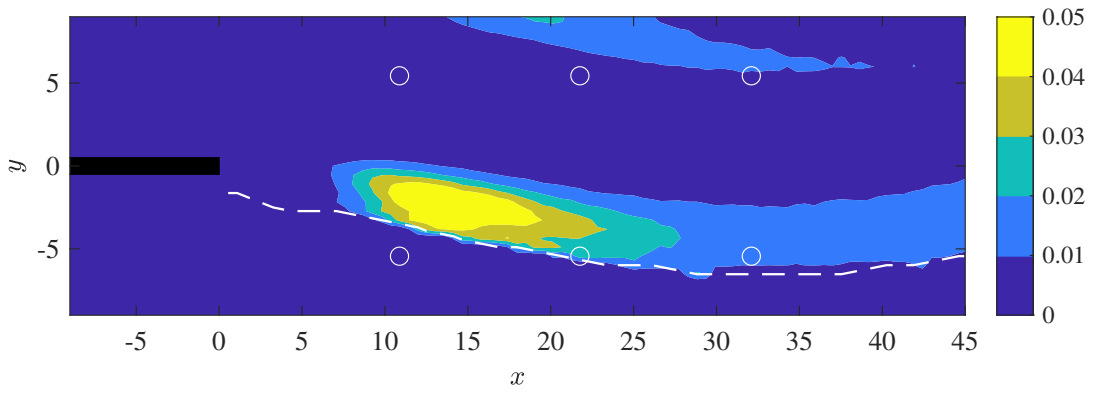

Fig. 6 Contour of $\overline{v'v'}/U_g^2$ of the HI-M case of Table 1. The splitter plate is highlighted in black, while the white dashed line denotes the time-averaged interface location. The white circles represent the monitoring locations where the PSD of unsteady velocity fluctuations is evaluated.

region is highlighted by the negative values of $\bar{u}$ for y around zero. Far from $y = 0$, the velocity profile is characterized by an almost uniform distribution in both air ($y > 2$) and water ($y < -1.1$) streams, while it undergoes strong spatial variations within the region $-1.1 < y < 2$. Downstream of the wake region, the velocity profile is influenced by the gas-gas mixing layer forming between the injected gas stream and the still ambient, with consequent reduction of the local $\bar{u}$ value by increasing y (phenomenon of jet expansion, see Descamps et al. [17]).

The gas Reynolds number Re_g effect on the mean flow topology is first shown in Fig. 4, which reports the velocity magnitude $\bar{V}$ contour maps for the LO, REF and HI cases, respectively in panels (a), (b) and (c). As Re_g increases, the momentum transferred by shear from the gas to the liquid stream clearly increases. Due to the sudden change of shear boundary condition downstream of the plate, the liquid velocity relaxes, and the water jet progressively accelerates and contracts along the streamwise direction x (Tillett [18]). Moreover, outside from the wake region, the gas jet progressively deviates downwards as Re_g increases, as also found in the numerical simulations performed by Agbaglah et al. [19]. The main finding regarding the time-averaged flow fields analysis is that the wake region progressively shortens by increasing the Reynolds number from the LO (a) to the HI (c) case, for which it vanishes. This aspect is further quantified in Fig. 5, where the trend $x_w(Re_g)$ is reported including more Reynolds number values; it can be seen that $x_w = 0$ for $Re_g = 768$.

IV. Unsteady flow development

The unsteady flow development is investigated in this section by computing the power spectral density (PSD) of the measured normal-to-flow velocity component fluctuations $v'(t) = v(t) - \bar{v}$, considering different streamwise x and normal-to-flow y locations in gas and liquid flows (white circles in Fig. 6).

We first focus the attention on the Re_g effect on the frequency spectra evaluated in gas flow (i.e. at $y = 5.44$) at three different streamwise stations, namely $x = 10.88$, 21.76 and 32.09. Results are reported in Fig. 7 for the LO (panels (a)-(c)), REF ((d)-(f)) and HI ((g)-(i)) cases, respectively. Note that, for each case, fluctuation amplitudes are made dimensionless by means of the corresponding value of gas injection velocity U_g, while frequencies are reduced with respect to the time scale $t_s = \delta_g/U_g$ (i.e. $St = f\delta_g/U_g$). At relatively low Reynolds number (LO case), the frequency spectra computed at different x stations are characterized by a high frequency content, the peak value being $St_p = O(10^{-2})$ ($f_p = 10^2$ Hz). Moreover, the specific value of St_p depends on the streamwise location x: it goes from $St_p = 0.05$ to $St_p = 0.02$ moving from $x = 10.88$ to $x = 32.09$ (Fig. 7(a)-(c)). On the other hand, when the Reynolds number increases up to $Re_g = 768$, the peak frequency shifts to lower values ($St_p = O(10^{-4})$, $f_p = O(1)$ Hz), which still slightly depend on the spatial location (it goes from $St_p = 2.0 \cdot 10^{-4}$ to $St_p = 3.5 \cdot 10^{-4}$ moving from panel (g) to (i)). Note that, being the time scale t_s employed to reduce the dimensional frequencies a decreasing function of Re_g, the St range reported in panels (g)-(i) is smaller than in previous panels of Fig. 7.

We explicitly note that findings discussed above are consistent with theoretical predictions based on local spatio-temporal stability analyses of the flow recently presented in literature (Fuster et al. [16], Otto et al. [20]). In particular, Otto et al. [20] pointed out that, at relatively low M and Re_g values, the two-phase mixing layer flow behaves like a noise amplifier, being characterized by convective instabilities. In this case, numerical simulations performed by Fuster

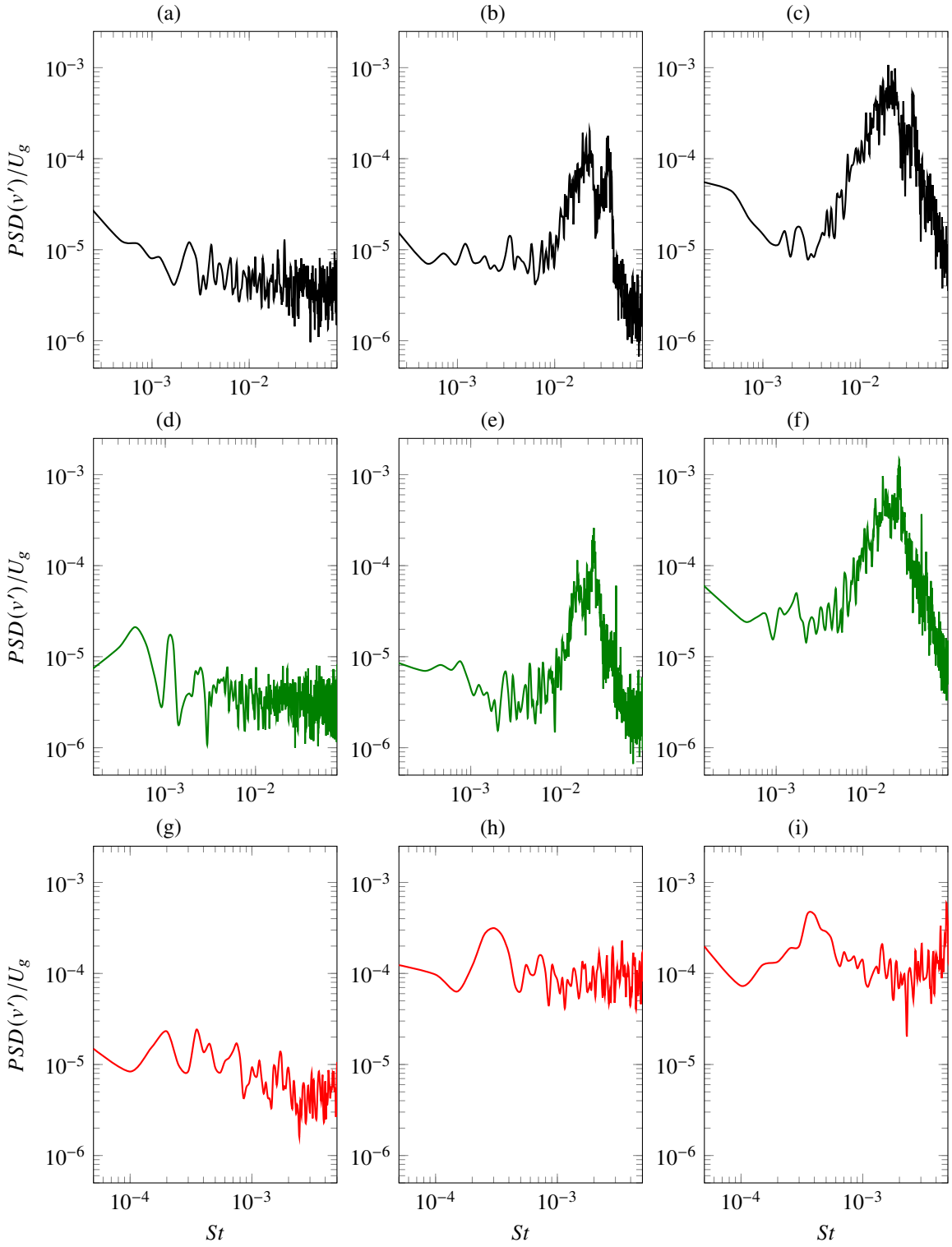

Fig. 7 Reynolds number Re_g effect on the PSD of normal-to-flow velocity component fluctuation $v'(t)/U_g$ at different streamwise x stations in gas flow (i.e., at $y = 5.44$): LO ((a)-(c)); REF ((d)-(f)); HI ((g)-(i)) cases of Table 1. From top to bottom: $x = 10.88$, 21.76, 32.09 (see also Fig. 6).

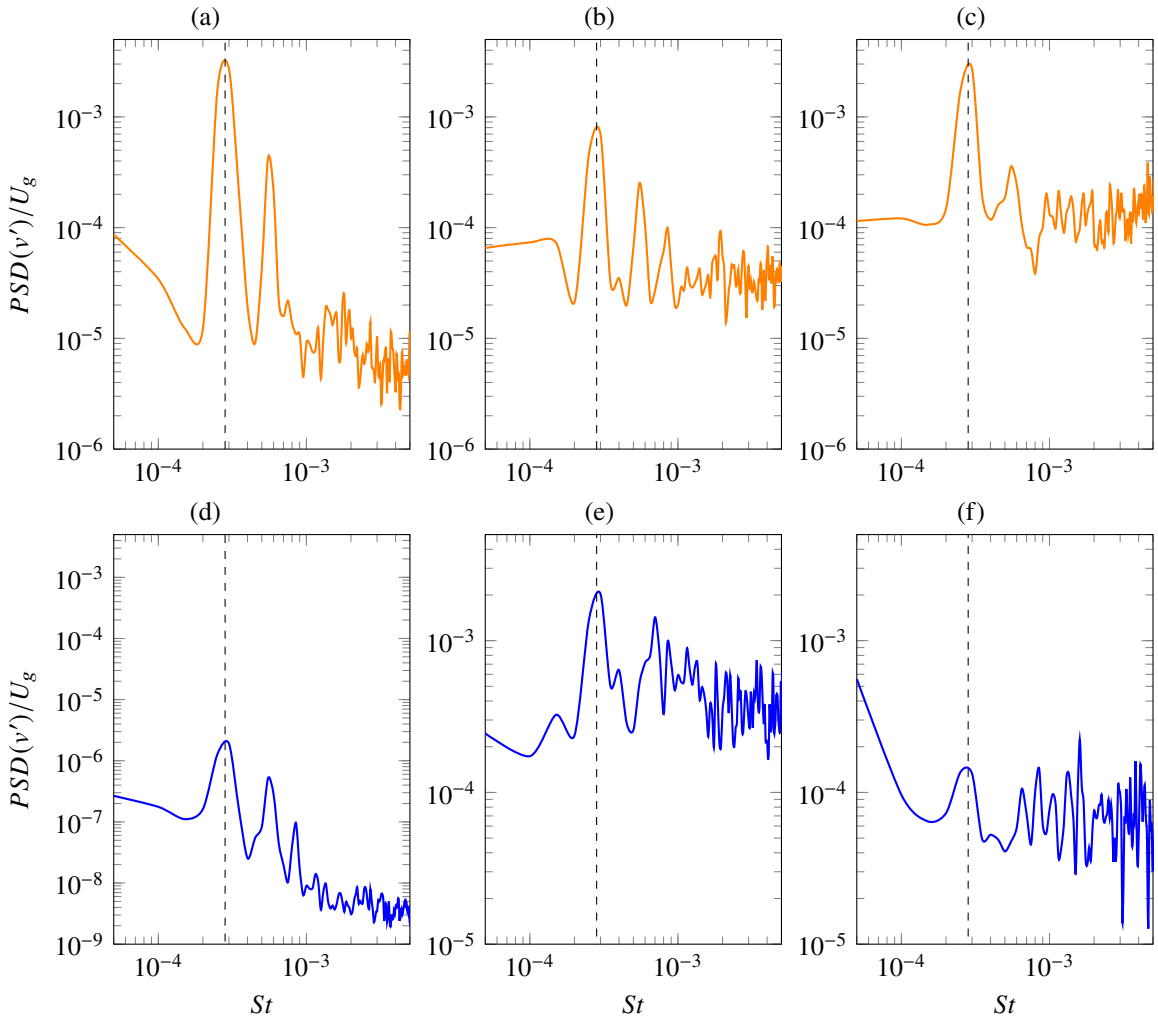

Fig. 8 PSD of $v'(t)/U_g$ at different (x, y) locations in gas ($y = 5.44$, orange curves) and water ($y = -5.44$, blue curves) flows: $x = 10.88$ (panels (a) and (d)), 21.76 (panels (b) and (e)), 32.09 (panels (c) and (f)), see also Fig. 6. The vertical dashed line in each panel denotes the peak reduced frequency $St_p = 2.8 \cdot 10^{-4}$. HI-M case of Table 1.

et al. [16] have shown that frequency spectra of the gas-liquid interface oscillatory dynamics strongly depend on the injected noise level (e.g. the turbulence fluctuations within the gas phase, characterized by high frequency values) and on the selected streamwise station. On the other hand, at relatively high Re_g, Otto et al. [20] and Fuster et al. [16] outlined a transition from convective to absolute instability of the flow when M increases beyond a critical threshold M_c ($M_c = O(1)$ for $\rho_g/\rho_l = 0.001$ in Fuster et al. [16]). In the latter case, the flow acts as an oscillator, driving the unsteady dynamics at a specific forcing frequency not related to the noise perturbations spectrum.

For the highest gas Reynolds number value here investigated ($Re_g = 768$), Fig. 8 reports the frequency spectra computed in both gas (orange curves) and liquid (blue curves) flows by further increasing the dynamic pressure ratio up to $M = 25.56$, which physically corresponds to reduce the liquid injection velocity U_l at fixed U_g (HI-M case of Table 1). The main result arising from the analysis of Fig. 8 is that, when the gas-liquid dynamic pressure ratio increases up to $M = 25.56$, the peak reduced frequency becomes independent on the specific spatial location (x,y), and it is equal to $St_p = 2.8 \cdot 10^{-4}$. It is found that, at high Re_g and M values, the velocity fluctuations are characterized by low frequency temporal oscillations synchronized over a large spatial extent of the flow field.

V. Conclusion

The wake-mixing layer flow developing past a splitter plate separating two parallel gas and liquid co-flowing currents has been experimentally investigated in this work. Time-resolved particle image velocimetry (TR-PIV) measurements of the two-phase velocity field have been performed simultaneously in gas and liquid streams, shedding light on both mean (time-averaged) and unsteady features of the flow configuration. A selected reference (REF) case has been first analyzed, revealing the presence of a wake region within the flow field, right behind the splitter plate. By progressively moving downstream along the streamwise x direction, a pure mixing layer region (namely absence of wake component) has been retrieved. The effect of two governing flow parameters, namely the gas Reynolds number Re_g and the gas-liquid dynamic pressure ratio M, has been then investigated, focusing first on the mean flow topology. It has been found that the streamwise extension of the wake x_w is a monotonic decreasing function of the gas Reynolds number, and it vanishes for the highest Re_g value considered (HI case), the two-phase flow resulting in a pure mixing layer regime. The unsteady flow development has been then characterized by means of the spectral analysis of normal-to-flow (i.e. along y direction) velocity fluctuating quantities $v'(t)$, performed in both gas and liquid flows. In the low Reynolds number configuration (LO case), it has been found that frequency spectra computed at different x stations are characterized by a high frequency content, the peak reduced frequency being $St_p = O(10^{-2})$ and its specific value depending on the streamwise location x. On the other hand, by progressively increasing Re_g (REF and HI cases), the peak reduced frequency shifts to lower values ($St_p = O(10^{-4})$), and it becomes independent on the specific spatial location (x,y) by further increasing M (HI-M case). It has been found that, at high Re_g and M values, velocity fluctuations are characterized by low frequency temporal oscillations synchronized over a large spatial extent of the flow field. The different regimes outlined by variation of the flow governing parameters have been found to be consistent with convective/absolute instability behaviors highlighted by spatio-temporal linear stability analyses of the flow recently presented in literature.

The experimental data here presented could be employed to perform a data-driven modal decomposition analysis of the two-phase mixing layer flow, with the aim of shedding light on the relationship between the measured velocity oscillations and the spatio-temporal dynamics of the gas-liquid interface in relevant flow conditions.

Acknowledgments

The stay of Alessandro Della Pia at Delft University of Technology was financially supported by University of Naples Federico II and Compagnia di San Paolo, in the framework of the STAR Program 2020. Theodoros Michelis and Marios Kotsonis were supported by the European Research Council (project #: 803082). The authors wish to thank S. Bernardy and E. Langedijk for sharing their technical knowledge during the experimental preparation.

References

[1] Raynal, L., Villermaux, E., Lasheras, J. C., and Hopfinger, E. J., "Primary instability in liquid-gas shear layers," *11th Symposum on Turbulent Shear Flows*, Vol. 3, 1997, pp. 27.1–27.5.

[2] Ben Rayana, F., Cartellier, A., and Hopfinger, E., "Assisted atomization of a liquid layer: investigation of the parameters affecting the mean drop size prediction," *Proceedings ICLASS 2006, August 27 - September 1, Kyoto Japan. Academic, iSBN4-9902774-1-4.*, 2006.

[3] Eggers, J., and Villermaux, E., "Physics of liquid jets," *Reports on Progress in Physics*, Vol. 71, No. 036601, 2008.

[4] Lefebvre, A. H., "Atomization and Sprays," *Emisphere Publishing*, 1989.

[5] Ling, Y., Fuster, D., Tryggvason, G., and Zaleski, S., "A two-phase mixing layer between parallel gas and liquid streams: multiphase turbulence statistics and influence of interfacial instability," *Journal of Fluid Mechanics*, Vol. 859, 2019, pp. 268–307.

[6] Jiang, D., and Ling, Y., "Impact of inlet gas turbulence on the formation, development and breakup of interfacial waves in a two-phase mixing layer," *Journal of Fluid Mechanics*, Vol. 921, No. A15, 2021.

[7] Bozonnet, C., Matas, J. P., Balarac, G., and Desjardins, O., "Stability of an air-water mixing layer: focus on the confinement effect," *Journal of Fluid Mechanics*, Vol. 933, No. A14, 2022, pp. 1–27.

[8] Marmottant, P., and Villermaux, E., "On spray formation," *Journal of Fluid Mechanics*, Vol. 498, 2004, pp. 73–111.

[9] Sanchis, A., and Jensen, A., "Dynamic masking of PIV images using Radon transform in free surface flows," *Experiments in Fluids*, Vol. 51, 2011, pp. 871–880.

[10] Ayati, A. A., Kolaas, J., Jensen, A., and Johnson, G. W., "A PIV investigation of stratified gas-liquid flow in a horizontal pipe," *International Journal of Multiphase Flow*, Vol. 61, 2014, pp. 129–143.

[11] Andrè, M. A., and Bardet, P. M., "Interfacial shear stress measurements using high spatial resolution multiphase PIV," *Experiments in Fluids*, Vol. 56, No. 132, 2015.

[12] Buckley, M. P., and Veron, F., "Airflow measurements at a wavy air-water interface using PIV and LIF," *Experiments in Fluids*, Vol. 58, No. 161, 2017.

[13] Kosiwczuk, W., Cessou, A., Trinitè, M., and Lecordier, B., "Simultaneous velocity field measurements in two-phase flows for turbulent mixing sprays by means of two-phase PIV," *Experiments in Fluids*, Vol. 39, 2005, pp. 895–908.

[14] Scarano, F., and Riethmuller, M. L., "Advances in iterative multigrid PIV image processing," *Experiments in Fluids*, Vol. 29, No. 7, 2000, pp. S051–S060.

[15] Westerweel, J., and Scarano, F., "Universal outlier detection for PIV data," *Experiments in Fluids*, Vol. 39, No. 6, 2005, p. 1096–1100.

[16] Fuster, D., Matas, J. P., Marty, S., Popinet, S., Hoepffner, J., Cartellier, A., and Zaleski, S., "Instability regimes in the primary breakup region of planar coflowing sheets," *Journal of Fluid Mechanics*, Vol. 736, 2013, pp. 150–176.

[17] Descamps, M., Matas, J., and Cartellier, A., "Gas-liquid atomisation: gas phase characteristics by PIV measurements and spatial evolution of the spray," *2nd colloque INCA, Initiative en Combustion Avancèe, Rouen: France.*, 2008.

[18] Tillett, J. P. K., "On the laminar flow in a free jet of liquid at high Reynolds numbers," *Journal of Fluid Mechanics*, Vol. 32, No. 2, 1968, pp. 273–292.

[19] Agbaglah, G., Chiodi, R., and Desjardins, O., "Numerical simulation of the initial destabilization of an air-blasted liquid layer," *Journal of Fluid Mechanics*, Vol. 812, 2017, pp. 1024–1038.

[20] Otto, T., Rossi, M., and Boeck, T., "Viscous instability of a sheared liquid-gas interface: Dependence on fluid properties and basic velocity profile," *Physics of Fluids*, Vol. 25, 2013, p. 032103.